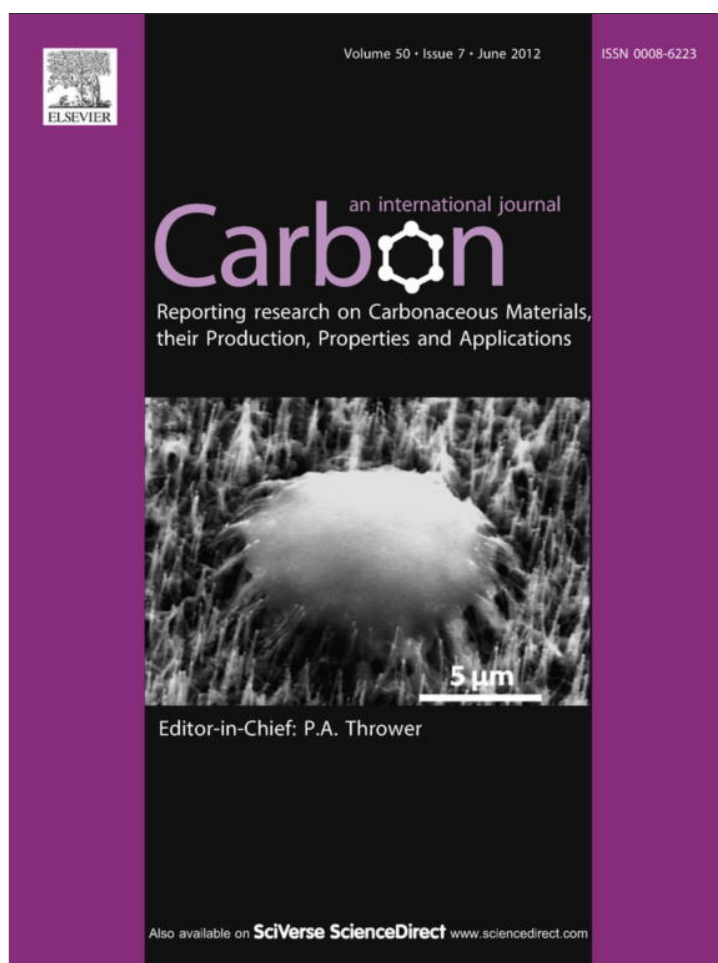


Provided for non-commercial research and education use.
Not for reproduction, distribution or commercial use.



This article appeared in a journal published by Elsevier. The attached copy is furnished to the author for internal non-commercial research and education use, including for instruction at the authors institution and sharing with colleagues.

Other uses, including reproduction and distribution, or selling or licensing copies, or posting to personal, institutional or third party websites are prohibited.

In most cases authors are permitted to post their version of the article (e.g. in Word or Tex form) to their personal website or institutional repository. Authors requiring further information regarding Elsevier's archiving and manuscript policies are encouraged to visit:

<http://www.elsevier.com/copyright>

Available at www.sciencedirect.com

SciVerse ScienceDirect

journal homepage: www.elsevier.com/locate/carbon

Synthesis and field emission properties of vertically aligned carbon nanotube arrays on copper

Suman Neupane ^a, Mauricio Lastres ^a, Melissa Chiarella ^a, Wenzhi Li ^{a,*}, Qingmei Su ^b, Gaohui Du ^b

^a Department of Physics, Florida International University, Miami, FL 33199, USA

^b Institute of Physical Chemistry, Zhejiang Normal University, Jinhua 321004, Zhejiang, China

ARTICLE INFO

Article history:

Received 14 October 2011

Accepted 8 February 2012

Available online 16 February 2012

ABSTRACT

We report the synthesis of periodic arrays of carbon nanotubes (CNTs) with different densities on copper substrate by employing nanosphere lithography (NSL) and plasma enhanced chemical vapor deposition. At a growth pressure of 8 torr and temperature of 520 °C, vertically aligned bamboo-like CNTs were formed with a catalyst particle on the tip. Electrical properties of CNTs with different densities were investigated for the possible applications in field emission (FE). The investigation of FE properties reveals a strong dependence on the density of CNTs. Experimental results show that NSL patterned low density CNTs exhibit better field emission properties as compared to the high density CNTs. Low-density CNTs exhibit lower turn-on and threshold electric fields, and a higher field enhancement factor. The high density of CNTs results in the deterioration of the FE properties due to the screening of the electric field by the neighboring CNTs.

© 2012 Elsevier Ltd. All rights reserved.

1. Introduction

Carbon nanotubes (CNTs) exhibit intriguing mechanical, electrical, optical, thermal, and electrochemical properties and have been extensively studied since the landmark paper by Iijima in 1991 [1]. CNTs are ideal candidates for field emission applications because of their high electrical and thermal conductivities, tremendous mechanical strength, and high aspect ratio [2–4]. CNTs have shown a potential for application in field emission displays, X-ray sources, lamps, microwave amplifiers, and nanoelectronics [5–9]. Many of these devices require the controlled growth of vertically aligned CNTs (VACNTs) directly on the conducting substrates. The CNTs synthesized by arc discharge and laser ablation methods are highly entangled and possess a lot of impurities [10]. The plasma enhanced chemical vapor deposition (PECVD) process has garnered an appropriate attention due to its ability to synthesize vertically

aligned CNT arrays at a predetermined position. It is also desirable to grow CNTs on metallic substrates like copper (Cu), which results in a lower contact resistance as compared to conventional CNTs grown on a silicon substrate. The ohmic contact between the CNTs and the metallic substrate ensures an easy electron transport, and the rigidity of these nanostructures enables the emitters to withstand high current during the process of emission. There have been efforts to produce high-performance CNT emitters by doping, plasma irradiation, thermal oxidation, laser pruning, metal coating, etc. [11–15].

However, it is also possible to enhance the emission properties of CNTs by varying the density of CNTs. A high-density array of CNTs results in the screening of the electric field by the neighboring CNTs and hence the reduction in the emission current, whereas the emission from a low density of CNTs is poor due to the availability of fewer number of emission sites. Selected area low-density growth of CNTs has been achieved

* Corresponding author: Fax: +1 305 348 6700.

E-mail address: Wenzhi.Li@fiu.edu (W. Li).

0008-6223/\$ - see front matter © 2012 Elsevier Ltd. All rights reserved.

doi:10.1016/j.carbon.2012.02.024

by patterning the catalyst using nanosphere lithography (NSL), electron beam lithography, photolithography, focused ion beam lithography, chemical etching, and others [16–21]. NSL is an inexpensive and efficient process to selectively pattern catalyst islands over which CNTs can be synthesized. A monolayer of polystyrene spheres (PS) of a specified diameter is used to create a mask over which the catalyst is deposited by e-beam evaporation, pulsed laser deposition, sputtering, etc. The PS layer is subsequently removed by wet chemical methods to obtain a honeycomb pattern of catalyst deposited in the interstices of the spheres. The size and spacing between these catalyst islands can be controlled by varying the diameter of spheres. Larger spheres result in bigger catalyst islands which are located further apart from each other as compared to the islands created by the smaller spheres. The VACNTs synthesized over these patterns exhibit better field emission behavior than the CNT thin films due to a decreased screening effect. In this study, we have employed PS of different diameters to grow CNTs of different densities on Cu substrates and used these CNTs to understand how the densities of CNTs govern the field emission properties.

There have been several reports on the theoretical simulation for the behavior of CNTs as efficient field emitters. Dionne et al. have performed a numerical investigation of the field enhancement factor of individual as well as array of CNTs [22]. It has been reported that CNT emitters have optimal total emission when the spacing between neighboring CNTs is on the order of twice their height. In an array consisting of CNTs with two different heights, there was no significant screening of the electric field when the taller CNTs were twice the height of shorter CNTs. Wang et al. have solved the Laplace equation for individual CNTs and for the hexagonal arrays of CNTs to understand the influence of intertube distance, anode–cathode distance and the structure of the tip on the field emission [23]. Considering the emission current density, the field emission can be optimal when the intertube distance of CNTs array is close to the CNTs height.

Although there have been reports of the synthesis of CNTs using Cu as catalysts [24,25], it is still challenging to grow well graphitized VACNTs directly over Cu substrates [26,27]. Duboscq et al. have synthesized VACNTs on 400 nm of Cu film on Si/SiO₂ with Ni as catalyst and TiN as a buffer layer using PECVD [28]. Banerjee et al. synthesized coiled carbon fibers on hydrogen-fluoride etched Cu substrates by PECVD [29]. Cu has fully filled 3d-orbitals, which prevents the formation of covalent bonds with hydrocarbon molecules. Also, the small binding energy of Cu with carbon subdues the process of graphitization. Furthermore, Cu has low carbon solubility preventing the saturation of carbon atoms required to form the CNT structures [30]. To overcome these problems, a thin buffer layer of Cr or TiN should be deposited on the Cu substrate prior to the deposition of Ni catalyst layer to ensure the synthesis and good adhesion of CNTs with the substrate. In this study, we have synthesized dense arrays of VACNTs on Cu substrates with a buffer layer of Cr using PECVD process. We have also employed NSL with polystyrene spheres of different diameters to pattern Ni catalyst dots on which VACNT patterns are grown. The dense VACNT array and the patterned VACNT arrays allow us to investigate how the variation in spacing between CNTs affects their field emission behavior

if the CNTs have a similar height. The growth of patterned CNTs on conducting substrates allows for the in situ fabrication of electron emitters capable of delivering stable currents under an appropriate vacuum. The enhancement of field emission by the post-growth treatment of the samples by different methods raises an incompatibility issue with the fabricated devices. Hence, it is more desirable to synthesize CNTs of specific density at a predetermined location.

2. Experimental

2.1. Nanosphere lithography

The catalyst pattern was prepared by a slight modification on the reported NSL procedures as follows [16]. An oxygen-free Cu plate (1 cm × 1 cm × 1 mm) was polished with sand paper to a smooth finish, and then it was ultrasonically cleaned in acetone and ethanol baths, each for 5 min. A 15 nm buffer layer of Cr was deposited on the Cu substrate using an e-beam evaporation system operated at room temperature. Clean silicon wafers 2 cm × 2 cm (donor substrates) were treated in RCA solution for 80 min. The RCA solution contains NH₄OH:H₂O₂:H₂O in the ratio 1:1:5 and was heated at 80 °C with donor substrates while the Cr coated Cu substrates (recipient substrates) were dipped in RCA solution for 10 s to render them hydrophilic. Commercially available (Spherotech Inc.) suspensions of PS (5% w/v) with diameters 0.5, 1.0, and 1.8 μm were used to create a monolayer in two steps, spin coating followed by dip coating. The PS suspensions were mixed with ethanol at a volume ratio of 1:7, 1:3, and 1:2 for spheres of diameter 0.5, 1.0, and 1.8 μm, respectively. The concentration of PS solution, for spheres of different diameters, was maintained at different levels to ensure the optimum areal coverage of the substrate without forming a multilayer. About 15–20 μl drops of the mixed solution were then dropped onto the hydrophilic donor substrate, followed by spinning the substrates at a speed of 700 rpm for 40 s. Next, we transferred the monolayer on the donor substrate onto a beaker containing deionized water. Finally, the floating monolayer was lifted off from the water surface by the recipient substrate. The combination of spin coating and dip coating facilitated the formation of a well ordered monolayer of PS on the recipient Cr-coated Cu substrate. A thin layer of 6.5 nm Ni was deposited on the PS patterned recipient substrate by e-beam evaporation system. The spheres were removed by sonication in ethanol to obtain a periodic array of Ni dots over the recipient substrate before the PECVD process.

2.2. CNT synthesis and electron microscopy

Vertically aligned CNT arrays were synthesized by PECVD process. The details of the synthesis procedure have been described elsewhere [31]. Briefly, a NSL patterned Cr-coated Cu substrate was loaded into a PECVD system and pumped down to 10⁻⁶ torr. For synthesizing CNTs, we used a mixture of C₂H₂ (30 sccm) as carbonaceous precursor and NH₃ (100 sccm) as diluting and etching gas. The substrate was heated to a temperature of 520 °C while NH₃ was introduced at a rate of 100 sccm until the pressure in the reaction chamber reached 8 torr. The power of the DC plasma was maintained at 70 W

while C_2H_2 was introduced. The synthesis time was 10 min for all experiments. The synthesized CNTs were allowed to cool naturally under high vacuum before further characterization. Surface morphology analysis of the CNT nanostructures was performed by a field emission scanning electron microscope (SEM, JEOL JSM-6330F) operated at an accelerating voltage of 15 kV. Transmission electron microscopy (TEM) images and high resolution TEM (HRTEM) images were obtained from a JEOL-2100F apparatus operated at an accelerating voltage of 200 kV. For the TEM analysis, the CNTs synthesized on the Cu substrate were removed and dispersed ultrasonically in ethanol and the solution was dropped on the carbon coated copper TEM grid.

2.3. Field emission measurement

The field emission measurements were carried out using a diode configuration inside a vacuum chamber at a pressure level of 10^{-7} torr. The separation between the anode and cathode was maintained at 400 μm . The emission current was measured by a Keithley 4200-SCS and the power was provided by a DC power supply (Matsusada AU-15P20). A multiple number of samples with CNTs of various densities were tested to ensure the repeatability and reliability of the obtained results.

3. Results and discussions

3.1. Nanosphere lithography

The interstices between three adjacent spheres in the PS monolayer allow a Ni deposit to form the hexagonal pattern of Ni catalyst. Assuming that the Ni catalyst takes quasi-triangular shape, the size and spacing between the Ni catalyst particles can be calculated [16]. Fig. 1a–c show schematics of the relative variation of catalyst size (d_a) and separation for the catalyst sites (d_s) of closely packed hexagonal structures formed by spheres of diameter 0.5, 1.0, and 1.8 μm , respectively. The site densities of quasi-triangular Ni catalyst dots can be expressed as $(2.3/D^2)$, where D is the diameter of the sphere. Similarly, the catalyst size is expressed as $d_a = 0.232D$ and their separation is $d_s = 0.577D$. The size of catalyst islands and catalyst separation increases with the increase of the sphere diameter whilst the site density decreases with the increase of the sphere diameter. The size and their separation of the catalyst islands formed using the spheres of diameter 1.0 and 1.8 μm increase by 100% and 260% compared to that of catalyst islands formed using 0.5 μm spheres. On the contrary, the respective site density of the catalyst islands formed using 1.0 and 1.8 μm spheres decreases by 75% and 92% as compared to the catalyst islands formed using spheres

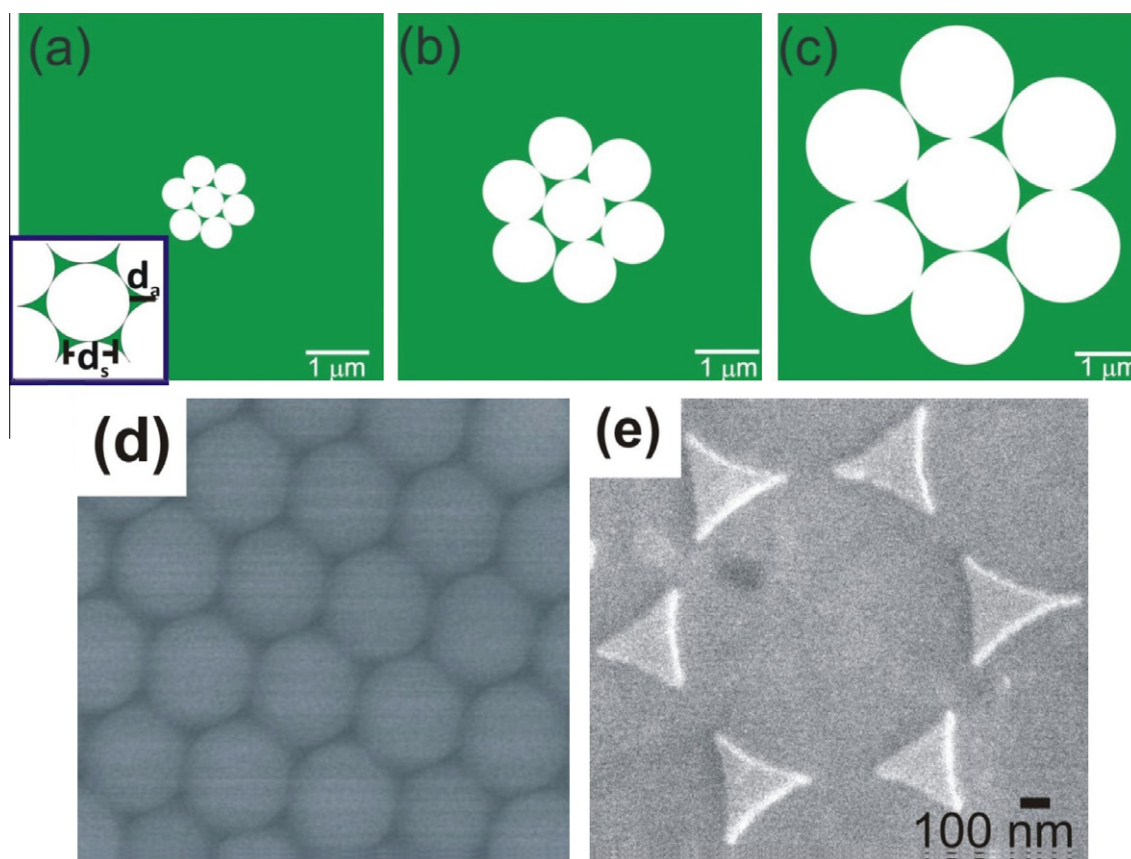


Fig. 1 – (a–c) The schematic of the relative variation of catalyst size (d_a) and separation for the catalyst sites (d_s) formed by spheres of diameter 0.5, 1.0, and 1.8 μm , respectively. Inset in Fig. 1a depicts the definitions of the catalyst size (d_a) and the separation of the catalyst sites (d_s). (d) SEM image of hexagonal pattern formed by a monolayer of spheres with diameter 1.0 μm . (e) SEM image of a well-ordered hexagonal array of quasi-triangular Ni catalyst particles after Ni deposition and removal of 1.0 μm PS spheres.

with diameter of 0.5 μm . The site density, size of a catalyst island, and the catalyst separation has been presented in Table 1 for spheres with different sizes. Fig. 1d shows the SEM image of a typical honeycomb structure of the PS mask formed by the spheres of diameter 1.0 μm . The Ni particles deposited through three adjacent spheres form hexagonal arrays of quasi-triangular catalyst sites as seen in Fig. 1e. The observed separation of the catalyst sites and their size distribution matches well with the theoretical predictions.

3.2. SEM analysis

The mechanism of CNT growth by a PECVD can be understood as follows: the thermal treatment reduces the thin film or quasi-triangular particles of catalyst into spherical dots. The energy available due to plasma generation and heating procedure decomposes the carbon precursors on the outer surface of the catalyst particles. The carbon atoms diffuse through the catalyst particles and tubular structures are formed with a catalyst particle either at the base or tip [10]. The plasma also helps to etch amorphous carbon that may deposit on top of the Ni particles, thus providing a steady supply of carbon atoms at the surface of the Ni particle [32].

Fig. 2a–d are the top view SEM images which show the distribution of the CNTs, whereas Fig. 2e–h offer a 45° tilt-view to show the alignment of individual CNTs. Compared to the high-density (HD) growth of CNTs on Ni catalyst film (note: without any catalyst pattern) (Fig. 2a), the CNTs synthesized with NSL patterned catalyst exhibit larger separation amongst each other (Fig. 2b–d). A careful observation of Fig. 2c and d reveals the growth of multiple numbers of CNTs from a single catalyst island. Similar growth behavior has been previously reported by Park et al. [33]. When the size of the catalyst island increases beyond the critical size of the Ni catalyst dot, a multiple number of CNTs will grow from a single catalyst island. During the annealing of catalyst, the Ni film from a single island disintegrates into a number of islands each of which act as a nucleation site for CNT growth. Similar reports of multiple growths of CNTs from a single island have been attributed to the low growth temperature of around 520 °C [34]. Different methods have been suggested to achieve the single growth of CNTs from a catalyst island. For example, deposition of a thinner layer of Ni catalyst, using spheres of smaller diameters, using a double layer PS mask for the catalyst deposition, chemical etching, etc. have been suggested as appropriate methods for the fabrication of a single CNT from a catalyst island. There have been reports of slight distortion of the CNTs from the original catalyst pattern due to migration of catalyst dot owing to their weak adhesion to the buffer layer [33]. However, no such noticeable migration of CNTs was observed in our experiments. The tilted-views in Fig. 2e–h show the formation of ver-

tically aligned CNTs. These CNTs have a length between 1–2 μm and diameter around 100 nm. The cluster of CNTs originating from a single catalyst island has a smaller separation as compared to CNTs from the adjacent islands. The aspect-ratio of these CNTs synthesized with different densities has similar values. However, these CNTs are expected to exhibit different field emission properties due to the variable proximity between the adjacent CNTs. Compared to the high-density CNTs on Ni film (without any catalyst pattern), CNTs grown on patterned catalyst dots using 0.5 μm spheres are expected to show better field enhancement properties. A further decrease in the density of CNTs grown on patterned catalyst dots using larger spheres might result in poor emission properties due to the presence of lower number of emitting sites. Hence, it is desirable to find the optimal density or separation of VACNTs (therefore optimal size of PS) to achieve the best field emission properties.

3.3. TEM analysis

The tubular structure of CNTs was verified by TEM observation. Fig. 3a shows the TEM image of the top portion of CNTs synthesized on Ni catalyst film, and Fig. 3b–d are the TEM images of CNTs grown from Ni catalyst dots formed with NSL using spheres of diameter 0.5, 1.0, and 1.8 μm , respectively (the corresponding SEM images are shown in Fig. 2a–h). We found that these multi-walled CNTs had a similar structure but slightly different lengths and diameter. The diameter of an individual CNT depends on the size of the catalyst fragment produced from a catalyst island. Smaller particles result in thinner tubes while bigger catalyst fragments result in thicker tubes. These CNTs have bamboo-like structures with a catalyst particle trapped at the tip suggesting a tip growth model. The graphitic planes in the tube walls are not always parallel to the tube axis but are often twisted and broken, which is the characteristic of CNTs synthesized by PECVD process [35]. The inset of Fig. 3a shows a magnified view of a typical CNT which contains a Ni catalyst rod forming a core-shell like structure. The effect of extrusion induced by the compressive force of the graphene layers during the growth of CNTs results in the formation of these core-shell structures. The Ni catalyst particle melts during the growth and a section of it may get trapped half way up the tube. At nanoscale dimensions, the melting point of metals can be significantly lower than that of their bulk counterparts [36]. Similar phenomenon of the melting of Ni catalyst at temperatures far below the melting point of bulk Ni has been reported earlier [37]. The inset in Fig. 3c shows the HRTEM image of a section of graphitic layers with the separation of about 0.34 nm which correspond to the separation of lattice planes (002) of graphite. The inset in Fig. 3d shows the interface between the graphitic planes of the CNT and the planes of the

Table 1 – The variation in site density, catalyst size and catalyst separation for spheres of different diameters.

Sphere size (μm)	Site density (per cm^2)	Catalyst size (μm)	Catalyst separation (μm)
0.5	9.2×10^8	0.116	0.289
1.0	2.3×10^8	0.232	0.577
1.8	0.7×10^8	0.418	1.039

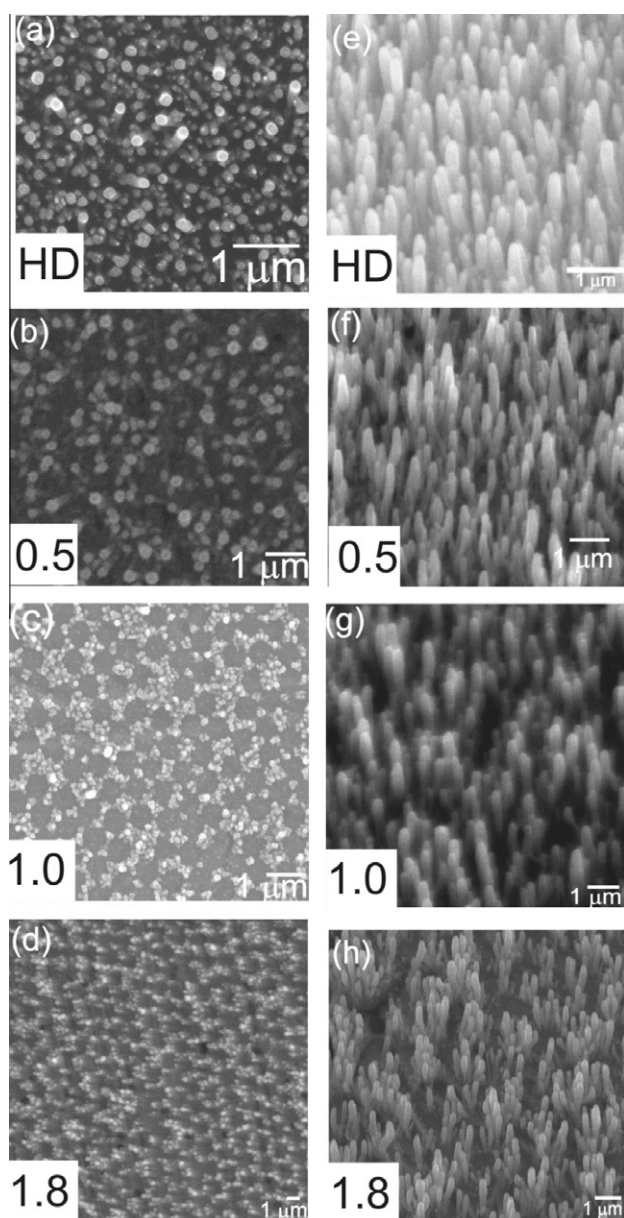


Fig. 2 – Variation of densities of CNTs prepared without and with different size PS. (a–d) are the SEM top-views of the CNTs; (e–h) are the tilt-views of the CNTs. Figures (a) and (e) are high-density CNTs grown on Ni film deposited without any NSL pattern. The numbers in the box on other images represent the diameter of spheres, in micrometers, used during the NSL.

Ni core in a core-shell structure. The parallel graphitic planes that make up the CNT are seen on the left part of the image in light contrast. The catalyst particle also exhibits crystalline structure with atomic planes separated by 0.18 nm corresponding to the Ni (200) lattice planes.

3.4. Field emission measurement

During the field emission measurements, the emission current was measured repeatedly at a particular applied volt-

age. Then the applied voltage was increased in steps of 200 V until the emission current saturated. The stability of the emission current was measured for a period of over 10 h. Finally, we repeated the field emission measurement several times for each of the CNT samples exposed to “electric annealing” to confirm the degree of repeatability of the emission characteristics. The field emission properties of the high density CNTs grown on Ni film and the low density CNTs grown on Ni dots patterned with the spheres of diameter 0.5, 1.0, and 1.8 μm are shown in Fig. 4. Fig. 4a shows the current density versus the electric field (F - J) curves of the CNTs with four different densities. All CNTs demonstrated excellent field emission properties with high current density and long stability. We define the turn-on electric field ($E_{\text{turn-on}}$) as the electric field required to obtain the emission current density of $1 \mu\text{A cm}^{-2}$ [38]. Similarly, the threshold electric field (E_{th}) is defined as the electric field corresponding to the emission current density of 1mA cm^{-2} . The numerical values of $E_{\text{turn-on}}$ and E_{th} for the four types of samples are presented in Table 2. The turn-on electric field for high-density CNTs was $7.96 \text{V } \mu\text{m}^{-1}$. The turn-on field decreased to 4.71, 6.41, and $5.19 \text{V } \mu\text{m}^{-1}$ for CNTs grown on catalyst dots patterned by spheres of diameter 0.5, 1.0, and 1.8 μm , respectively. Also, the threshold electric fields for CNTs with catalyst patterned by spheres of diameter 0.5, 1.0, and 1.8 μm are 8.71, 11.48, and $9.89 \text{V } \mu\text{m}^{-1}$, respectively. It is noteworthy that, for high-density CNTs, the emission current density of 1mA cm^{-2} could not be achieved even after increasing the applied electric field to $13.5 \text{V } \mu\text{m}^{-1}$. The lower values of turn-on field and threshold electric field clearly suggest that the low-density CNTs synthesized by the catalyst patterned by NSL are more favorable than the high-density growth for the optimum emission current. In the high density CNT arrays grown on Ni catalyst film, some of the emitted electrons will be trapped by the adjacent CNTs and only the CNTs emitted from the tip can contribute to the total current. There is a smaller probability of capturing emitted electrons in the case of low-density growth than in the high-density growth. This will increase the flux of electrons reaching the anode. Hence, the CNTs synthesized on catalyst patterned by spheres of different diameters exhibit better field emission properties than CNTs synthesized on Ni film [35]. The trapping of the electrons and screening of the electric field can be reduced in a low-density array of CNTs. The CNTs grown on catalyst patterned by NSL using spheres of 0.5 μm diameter had the lowest E_{th} and $E_{\text{turn-on}}$ among the low-density CNTs. The increase in total current despite the lower density indicates that an individual CNT emits more electrons when the CNTs are sparsely distributed. The further decrease in the site density of CNTs by using spheres of 1.0 μm diameter resulted in the reduction in emission current due to fewer number of CNTs. However, the CNTs grown from catalyst patterned by NSL using spheres of diameter 1.8 μm showed improved emission characteristics than those CNTs grown from catalyst patterned by NSL using spheres of diameter 1.0 μm . As evident from the SEM images, the CNTs grown from catalyst patterned by NSL using spheres of diameter 1.8 μm produces more CNTs from a single island as compared to CNTs grown from catalyst patterned by NSL using spheres of diameter 1.0 μm . The presence of a more number of CNTs within a single bundle contributes to the

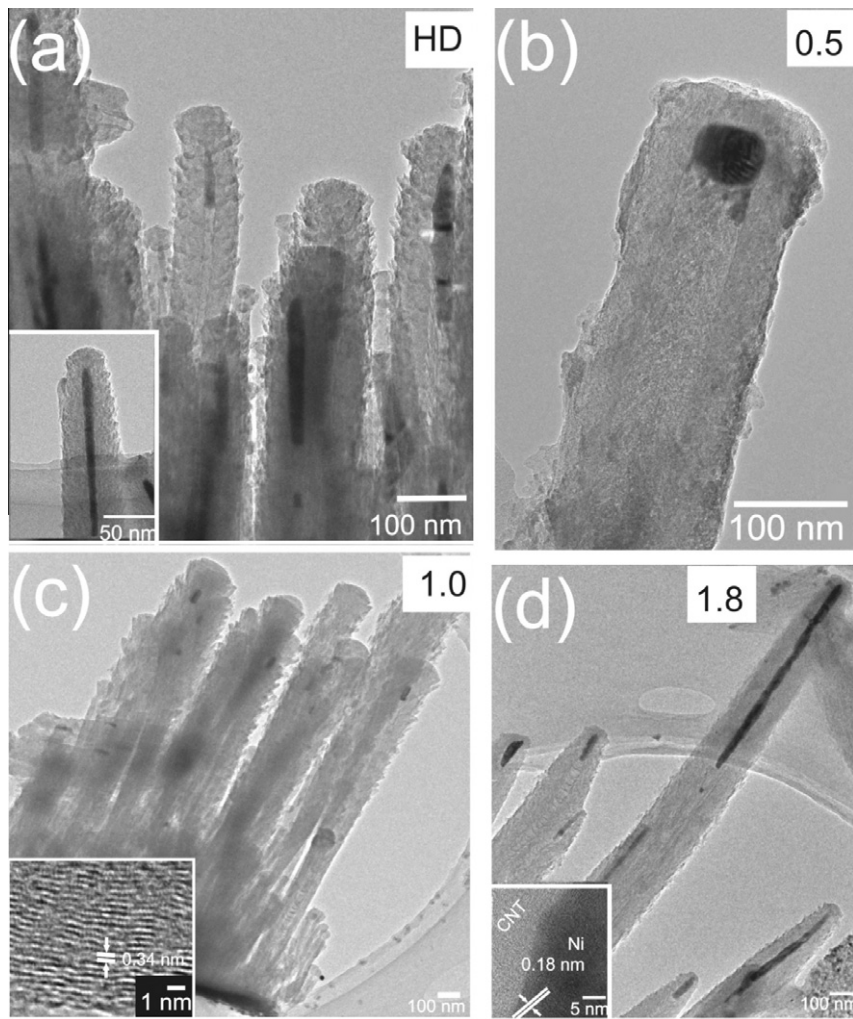


Fig. 3 – TEM images of the CNTs. (a) TEM image of high density CNTs grown on Ni film catalyst; (b–d) TEM images of CNTs synthesized on Ni catalyst dots patterned using spheres of diameter 0.5, 1.0, and 1.8 μm , respectively. The inset in (a) shows a rod-like Ni catalyst inside a CNT almost forming a core–shell structure. The inset in (c) shows the lattice fringes of graphitic planes in a single CNT. The inset in (d) shows the interface between the CNT and the Ni catalyst trapped inside the CNT.

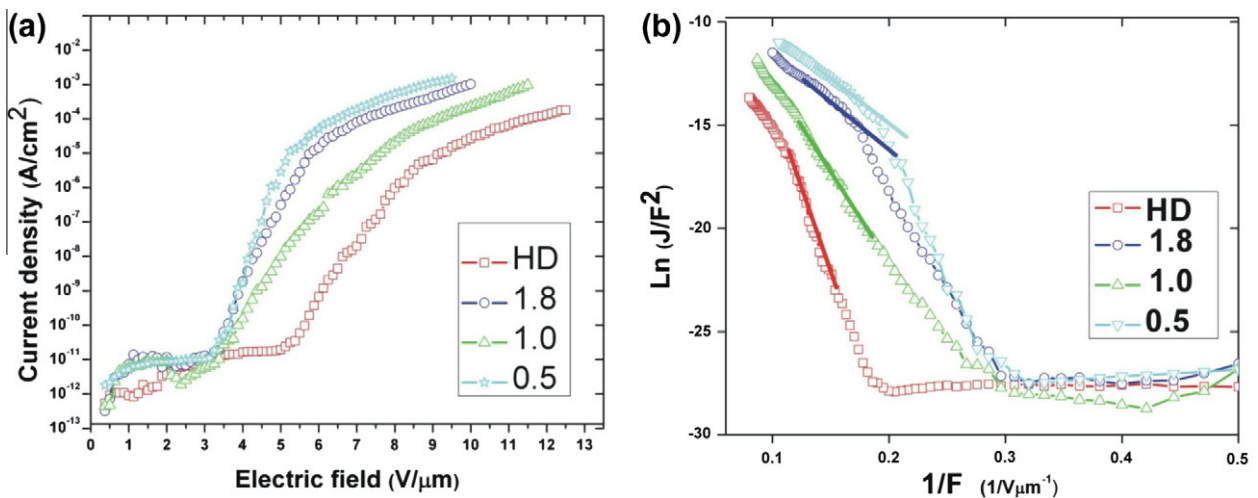


Fig. 4 – Field emission properties of CNTs with different densities. (a) F–J plot and (b) Fowler–Nordheim (F–N) plots.

Table 2 – Turn-on and threshold electrical fields of CNTs with different densities.

	High density	0.5 μm	1.0 μm	1.8 μm
$E_{\text{turn-on}}$ ($\text{V } \mu\text{m}^{-1}$)	7.96	4.71	6.41	5.19
E_{th} ($\text{V } \mu\text{m}^{-1}$)	NA	8.71	11.48	9.89
Field enhancement factor (β)	460	1760	855	1680

better performance of the emitters. Fuji et al. [39] performed a computer simulation to compare the resultant electric field due to a CNT bundle and a flat film of CNTs. It was found that electric field of the flat film is constant all over the emitter surface, whereas the electric field of the bundle is significantly higher at the edge than at the center. Hence, the electric field is predominantly concentrated along the circumference of the bundle which results in more emission sites. Thus CNTs synthesized from catalyst patterned using spheres of diameter 1.8 μm exhibited better emission current than the CNTs grown from catalyst patterned using spheres of diameter 1.0 μm due to the edge effect.

Fig. 4b shows the corresponding Fowler–Nordheim (F–N) plots for the CNTs with four different densities. The straight lines indicate the quantum mechanical tunneling characteristic of field electron emission. The field enhancement factor can be calculated using the F–N equation:

$$J = \left(\frac{A\beta^2 F^2}{\phi} \right) \exp \left(- \frac{B\phi^3}{\beta F} \right)$$

where J is the emission current density, $A = 1.56 \times 10^{-6} \text{ A V}^{-2} \text{ eV}$, $B = 6.83 \times 10^9 \text{ eV}^{-3/2} \text{ V m}^{-1}$ [40], β is the field enhancement factor, ϕ is the work-function, and F is the applied electric field. Assuming the work function of the MWCNTs to be 5.0 eV [41,42], the field enhancement factor can be calculated from the slope of the F–N plot. It is reported that the work-function of CNTs reduces to values of 3.0 eV and 2.0 eV at higher applied fields of 10 $\text{V } \mu\text{m}^{-1}$ and 14 $\text{V } \mu\text{m}^{-1}$, respectively [43]. The work-function of CNTs also depends on the presence of amorphous carbon material on the surface, presence of open-ended tube or closed-ended tube, presence of catalyst particle on the tubes, defects and others. Here in this study, we use $\phi = 5.0 \text{ eV}$ to make the comparison of the emission behavior of the various CNT arrays easier and simple. Hence, in Fig. 4b, we only consider the region where the work function does not decrease significantly below 5.0 eV and measure the slope of the straight lines as shown in Fig. 4b to estimate β . The field enhancement factors for high density CNTs and NSL patterned CNTs with spheres of diameter 0.5, 1.0, and 1.8 μm were 460, 1760, 855, and 1680, respectively. It is noteworthy that the experimental β is greater than geometrical β (the ratio of length to radius) of the CNTs by an order of magnitude. These large discrepancies between the β estimated from the F–N plots and geometrical $\beta \sim 50$ indicate that there are other mechanisms, in addition to quantum tunneling, for the field emission process [35]. The field emission properties depend upon the morphology of CNTs, structure of CNTs emitter and the method employed to measure the emission current. The ohmic contact between the CNTs and the substrate along with the vertical alignment of CNTs play an important role in the field emission. During the process

of field emission, the electrons should cross the interface between substrate and barrier layer, pass through CNTs, and finally emit into the vacuum. The contact resistance is lower for CNTs synthesized on conducting substrates than for the CNTs synthesized with buffer layer of SiO_2 , the low contact resistance will assist the process of field emission. The presence of the buffer layer of Cr in our samples ensures a robust contact of CNTs with the substrate over an extended period of emission time. Further, the low contact resistance between CNTs and Cr (1 k Ω) facilitates the electron transfer from the substrate to the CNTs during the emission [44].

Fig. 4b illustrates two distinct slopes on the F–N plots. The slope of F–N plots in the region of high electric field is lower as compared to the slope in the region of low electric field. Similar behavior has been attributed to vacuum space charge effects, changes in local density of states at the emitter's tip, interaction among adjacent tubes, solid-state transport, and adsorption and desorption of gaseous species even at high vacuum as a result of emission-assisted surface reaction process [45]. Although, it has been demonstrated that Murphy and Good theory better explains the emission phenomenon at high electric field in the range of $10^{7-10} \text{ V m}^{-1}$ and temperature of 1000–5000 K [46–48], we estimate that F–N equation is still applicable to explain the field emission in these experiments as such local temperatures on the CNT tip might have not been achieved. In this notion, we believe that the localized tip-cooling during field emission is partially responsible to compensate for the Joule heating [46].

3.5. Stability test

The stability of emission current is one of the most important parameters used to estimate the feasibility of CNT emitters for various application purposes. Fig. 5 shows the field emission stability of emission current from CNTs with different densities during the stability test. The initial emission current was set at the maximum value for the particular sample and the applied voltage was kept constant for 10 h. Only a small degradation in the emission current was observed when the CNTs were subjected to such a stringent current over a long period of time. The critical current from an individual CNT increases with its diameter. The CNTs with diameters in the range of 5–20 nm have the critical current in the range of 2–15 μA while CNTs with diameters of about 30 nm deliver the current in the range of 40–250 μA [49]. Wei et al. performed in situ TEM on the degradation of a CNT emitter and observed that CNTs suffered abrupt breaking at the point where the temperature reached a maximum value [50]. The CNTs in the present work have diameters in the range of 80–100 nm and are expected to withstand greater current preventing thermal degradation. The high thermal conductivity of both

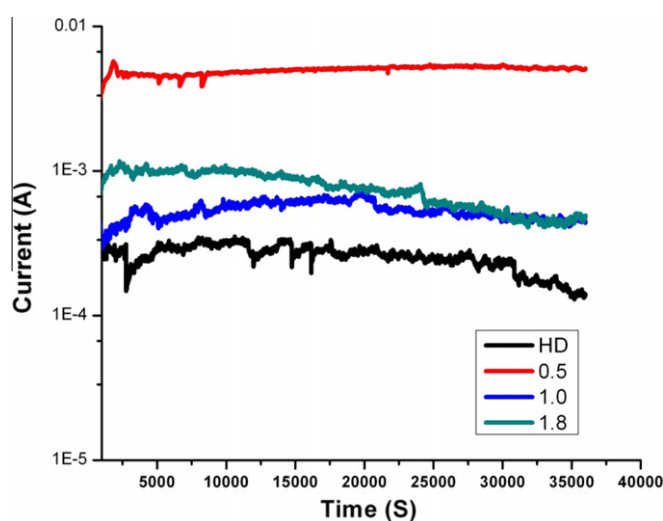


Fig. 5 – Field emission stability of CNT arrays with different densities.

the CNTs and the Cu substrate allows an unobstructed transfer of heat preventing the occurrence of high temperatures and destruction of the emitters. This will minimize the degradation of CNT emitters subjected to withstand the high temperature caused by Joule heating. Pandey et al. have simulated the electrical field for arrays having bundles of CNTs at different sites [51]. The maximum local electric field at the bundle is two-order of magnitude lower than those for rectangular arrays of CNTs. This will result in lower thermal and mechanical stress introduced on CNT bundles. We attribute the high field emission stability of our samples to the strong adhesion of CNTs with the Cu substrate, higher critical current and lowered stress. CNTs synthesized with the catalyst patterned by spheres of diameter of 1.8 μm exhibited a sharper decline in emission current over the test period as compared to other samples. The individual CNTs on samples with catalyst patterned by spheres of diameter 1.8 μm were liable to produce more current, due to a lower density than the CNTs on other samples, and were prone to quicker degradation.

4. Conclusions

Vertically aligned CNTs were synthesized on copper substrates with Ni catalyst nanodots patterned by nanosphere lithography. The density and location of CNTs were determined by the diameter of spheres. The as-synthesized CNTs followed a tip-growth mechanism with the Ni catalyst forming almost a core-shell like structure several nanometers long in many cases. The low-density growth of CNTs and the inherent decrease in contact resistance with the choice of metal substrate were favorable for the process of field emission. Among the high-density CNTs grown on Ni catalyst film and low-density CNTs grown on NSL patterned Ni catalyst dots, low-density CNTs synthesized on catalyst dots patterned from spheres of diameter 0.5 μm exhibited the best field emission properties in terms of lower turn-on and threshold fields, higher field enhancement, and longer stability. These results could facilitate the direct fabrication of

more cost-effective and site-selective CNT structures compatible with novel nanoelectronic devices.

Acknowledgment

W.Z. Li acknowledges the support by the National Science Foundation under grant DMR-0548061.

REFERENCES

- [1] Iijima S. Helical microtubules of graphitic carbon. *Nature* 1991;354(6348):56–8.
- [2] Berber S, Kwon YK, Tomanek D. Unusually high thermal conductivity of carbon nanotubes. *Phys Rev Lett* 2000;84(20):4613–6.
- [3] Treacy MMJ, Ebbesen TW, Gibson JM. Exceptionally high Young's modulus observed for individual carbon nanotubes. *Nature* 1996;381(6584):678–80.
- [4] Tans SJ, Devoret MH, Dai HJ, Thess A, Smalley RE, Geerligs LJ, et al. Individual single-wall carbon nanotubes as quantum wires. *Nature* 1997;386(6624):474–7.
- [5] Wang QH, Setlur AA, Lauerhaas JM, Dai JY, Seelig EW, Chang RPH. A nanotube-based field-emission flat panel display. *Appl Phys Lett* 1998;72(22):2912–3.
- [6] Lee NS, Chung DS, Han IT, Kang JH, Choi YS, Kim JM, et al. Application of carbon nanotubes to field emission displays. *Diamond Relat Mater* 2001;10(2):265–70.
- [7] Yue GZ, Qiu Q, Gao B, Cheng Y, Zhang J, Shimoda H, et al. Generation of continuous and pulsed diagnostic imaging X-ray radiation using a carbon-nanotube-based field-emission cathode. *Appl Phys Lett* 2002;81(2):355–7.
- [8] de Jonge N, Lamy Y, Schoots K, Oosterkamp TH. High brightness electron beam from a multi-walled carbon nanotube. *Nature* 2002;420(6914):393–5.
- [9] Milne WI, Teo KBK, Minoux E, Groening O, Gangloff L, Hudanski L, et al. Aligned carbon nanotubes/fibers for applications in vacuum microwave amplifiers. *J Vac Sci Technol B* 2006;24(1):345–8.
- [10] Meyyappan M, Delzeit L, Cassell A, Hash D. Carbon nanotube growth by PECVD: a review. *Plasma Sources Sci Technol* 2003;12(2):205–16.

- [11] Charlier JC, Terrones M, Baxendale M, Meunier V, Zacharia T, Rupesinghe NL, et al. Enhanced electron field emission in B-doped carbon nanotubes. *Nano Lett* 2002;2(11):1191–5.
- [12] Ahn KS, Kim JS, Kim CO, Hong JP. Non-reactive rf treatment of multiwall carbon nanotube with inert argon plasma for enhanced field emission. *Carbon* 2003;41(13):2481–5.
- [13] Zeng BQ, Xiong GY, Chen S, Wang WZ, Wang DZ, Ren ZF. Enhancement of field emission of aligned carbon nanotubes by thermal oxidation. *Appl Phys Lett* 2006;89(22):223119–1–3.
- [14] Cheng HF, Hsieh YS, Chen YC, Lin IN. Laser irradiation effect on electron field emission properties of carbon nanotubes. *Diamond Relat Mater* 2004;13(4–8):1004–7.
- [15] Liu C, Kim KS, Baek J, Cho Y, Han S, Kim SW, et al. Improved field emission properties of double-walled carbon nanotubes decorated with Ru nanoparticles. *Carbon* 2009;47(4):1158–64.
- [16] Huang ZP, Carnahan DL, Rybczynski J, Giersig M, Sennett M, Wang DZ, et al. Growth of large periodic arrays of carbon nanotubes. *Appl Phys Lett* 2003;82(3):460–2.
- [17] Teo KBK, Lee SB, Chhowalla M, Semet V, Binh VT, Groening O, et al. Plasma enhanced chemical vapour deposition carbon nanotubes/nanofibres – how uniform do they grow? *Nanotechnology* 2003;14(2):204–11.
- [18] Kim DH, Cho DS, Jang HS, Kim CD, Lee HR. The growth of freestanding single carbon nanotube arrays. *Nanotechnology* 2003;14(12):1269–71.
- [19] Wu J, Eastman M, Gutu T, Wyse M, Jiao J, Kim SM, et al. Fabrication of carbon nanotube-based nanodevices using a combination technique of focused ion beam and plasma-enhanced chemical vapor deposition. *Appl Phys Lett* 2007;91(17):173122–1–3.
- [20] Lee CJ, Kim DW, Lee TJ, Choi YC, Park YS, Lee YH, et al. Synthesis of aligned carbon nanotubes using thermal chemical vapor deposition. *Chem Phys Lett* 1999;312(5–6):461–8.
- [21] Tu Y, Lin YH, Ren ZF. Nanoelectrode arrays based on low site density aligned carbon nanotubes. *Nano Lett* 2003;3(1):107–9.
- [22] Dionne M, Coulombe S, Meunier JL. Screening effects between field-enhancing patterned carbon nanotubes: a numerical study. *IEEE Electron Dev* 2008;55(6):1298–305.
- [23] Wang XQ, Wang M, Ge HL, Chen Q, Xu YB. Modeling and simulation for the field emission of carbon nanotubes array. *Physica E* 2005;30(1–2):101–6.
- [24] Shaikjee A, Franklyn PJ, Coville NJ. The use of transmission electron microscopy tomography to correlate copper catalyst particle morphology with carbon fiber morphology. *Carbon* 2011;49(9):2950–9.
- [25] Zhou WW, Han ZY, Wang JY, Zhang Y, Jin Z, Sun X, et al. Copper catalyzing growth of single-walled carbon nanotubes on substrates. *Nano Lett* 2006;6(12):2987–90.
- [26] Talapatra S, Kar S, Pal SK, Vajtai R, Ci L, Victor P, et al. Direct growth of aligned carbon nanotubes on bulk metals. *Nat Nanotechnol* 2006;1(2):112–6.
- [27] Wang BA, Liu XY, Liu HM, Wu DX, Wang HP, Jiang JM, et al. Controllable preparation of patterns of aligned carbon nanotubes on metals and metal-coated silicon substrates. *J Mater Chem* 2003;13(5):1124–6.
- [28] Dubosc M, Casimirius S, Besland MP, Cardinaud C, Granier A, Duvail JL, et al. Impact of the Cu-based substrates and catalyst deposition techniques on carbon nanotube growth at low temperature by PECVD. *Microelectron Eng* 2007;84(11):2501–5.
- [29] Banerjee D, Jha A, Chattopadhyay KK. Efficient field emission from coiled carbon nano/microfiber on copper substrate by dc-PECVD. *Appl Surf Sci* 2010;256(24):7516–21.
- [30] Mata D, Amaral M, Fernandes AJS, Oliveira FJ, Costa PMFJ, Silva RF. Self-assembled cones of aligned carbon nanofibers grown on wet-etched Cu foils. *Carbon* 2011;49(7):2181–96.
- [31] Ren ZF, Huang ZP, Xu JW, Wang JH, Bush P, Siegal MP, et al. Synthesis of large arrays of well-aligned carbon nanotubes on glass. *Science* 1998;282(5391):1105–7.
- [32] Hofmann S, Ducati C, Robertson J, Kleinsorge B. Low-temperature growth of carbon nanotubes by plasma-enhanced chemical vapor deposition. *Appl Phys Lett* 2003;83(1):135–7.
- [33] Park KH, Lee S, Koh KH, Lacerda R, Teo KBK, Milne WI. Advanced nanosphere lithography for the areal-density variation of periodic arrays of vertically aligned carbon nanofibers. *J Appl Phys* 2005;97(2):024311–1–4.
- [34] Houweling ZS, Verlaan V, ten Grotenhuis GT, Schropp REI. Formation of isolated carbon nanofibers with hot-wire CVD using nanosphere lithography as catalyst patterning technique. *Thin Solid Films* 2009;517(12):3566–9.
- [35] Chhowalla M, Ducati C, Rupesinghe NL, Teo KBK, Amaratunga GAJ. Field emission from short and stubby vertically aligned carbon nanotubes. *Appl Phys Lett* 2001;79(13):2079–81.
- [36] Buffat P, Borel JP. Size effect on the melting temperature of gold particles. *Phys Rev A* 1976;13(6):2287–98.
- [37] Abdi Y, Koohsorkhi J, Derakhshandeh J, Mohajerzadeh S, Hoseinzadegan H, Robertson MD, et al. PECVD-grown carbon nanotubes on silicon substrates with a nickel-seeded tip-growth structure. *Mater Sci Eng C* 2006;26(5–7):1219–23.
- [38] Chen GH, Shin DH, Iwasaki T, Kawarada H, Lee CJ. Enhanced field emission properties of vertically aligned double-walled carbon nanotube arrays. *Nanotechnology* 2008;19(41):415703–1–6.
- [39] Fujii S, Honda S, Machida H, Kawai H, Ishida K, Katayama M, et al. Efficient field emission from an individual aligned carbon nanotube bundle enhanced by edge effect. *Appl Phys Lett* 2007;90(15):153108–1–3.
- [40] de Jonge N, Allieux M, Doytcheva M, Kaiser M, Teo KBK, Lacerda RG, et al. Characterization of the field emission properties of individual thin carbon nanotubes. *Appl Phys Lett* 2004;85(9):1607–9.
- [41] Groning O, Kuttel OM, Emmenegger C, Groning P, Schlappbach L. Field emission properties of carbon nanotubes. *J Vac Sci Technol B* 2000;18(2):665–78.
- [42] Huang BR, Lin TC, Chu JP, Chen YC. Long-term stability of a horizontally-aligned carbon nanotube field emission cathode coated with a metallic glass thin film. *Carbon* 2012;50(4):1619–24.
- [43] Zheng X, Chen GH, Li ZB, Deng SZ, Xu NS. Quantum-mechanical investigation of field-emission mechanism of a micrometer-long single-walled carbon nanotube. *Phys Rev Lett* 2004;92(10):106803–1–4.
- [44] Lim SC, Jang JH, Bae DJ, Han GH, Lee S, Yeo IS, et al. Contact resistance between metal and carbon nanotube interconnects: effect of work function and wettability. *Appl Phys Lett* 2009;95(26):264103–1–3.
- [45] Rakhi RB, Reddy ALM, Shaijumon MM, Sethupathi K, Ramaprabhu S. Electron field emitters based on multiwalled carbon nanotubes decorated with nanoscale metal clusters. *J Nanopart Res* 2008;10(1):179–89.
- [46] Dionne M, Coulombe S, Meunier JL. Energy exchange during electron emission from carbon nanotubes: considerations on tip cooling effect and destruction of the emitter. *Phys Rev B* 2009;80(8):085429–1–085429–10.
- [47] Dionne M, Coulombe S, Meunier JL. Field emission calculations revisited with Murphy and Good theory: a new interpretation of the Fowler–Nordheim plot. *J Phys D Appl Phys* 2008;41(24):245304–1–8.
- [48] Coulombe S, Meunier JL. Thermo-field emission: a comparative study. *J Phys D Appl Phys* 1997;30(5):776–80.
- [49] Doytcheva M, Kaiser M, de Jonge N. In situ transmission electron microscopy investigation of the structural changes

- in carbon nanotubes during electron emission at high currents. *Nanotechnology* 2006;17(13):3226–33.
- [50] Wei W, Liu Y, Wei Y, Jiang KL, Peng LM, Fan SS. Tip cooling effect and failure mechanism of field-emitting carbon nanotubes. *Nano Lett* 2007;7(1):64–8.
- [51] Pandey A, Prasad A, Moscatello J, Ulmen B, Yap YK. Enhanced field emission stability and density produced by conical bundles of catalyst-free carbon nanotubes. *Carbon* 2010;48(1):287–92.